Dynamic Stability of High-Drag Planetary Entry Vehicles at Transonic Speeds

WAYNE J. MARKO*
Jet Propulsion Laboratory, Pasadena, Calif.

The transonic dynamic stability of one 70° and two 60° half-angle cone configurations has been investigated in a continuous flow wind tunnel using free-flight techniques. The parameters varied were Mach number and oscillation amplitude for the approximate ranges of 0.6 to 2.0 and 0° to 15°, respectively. The test data show two marked effects: 1) a decrease in dynamic stability at transonic speeds relative to that exhibited in the subsonic and supersonic regimes, and 2) transonic dynamic stability data sensitive to oscillation amplitude. Generally, measured coefficients were destabilizing for angles of attack less than 10° and stabilizing at greater amplitudes. The effect of using these data in a six-degree-of-freedom computer program to generate oscillation envelopes and corresponding dynamic stability data for a simulated Mars entry trajectory is demonstrated.

Nomenclature

A = model reference area, $\pi d^2/4$
c.g. = center of gravity; distance to c. g. from physical model nose
C_D = (drag force)/$q_\infty A$; $C_{D_0} = C_D$ at $\alpha = 0$
C_L = (lift force)/$q_\infty A$; $C_{L_\alpha} = C_L$ slope/rad
C_m = (pitching moment) $q_\infty Ad$; $C_{m_\alpha} = C_m$ slope/rad
$\overline{C_{m_q}}$ = $\{C_{m_q} + C_{m_{\dot\alpha}}\}$ = dynamic stability coefficient (assumed constant over an oscillation cycle) $[\partial C_m/\partial(qd/V) + \partial C_m/\partial(\dot\alpha d/V)]$/rad
d = reference length, model diameter
I = model moment of inertia about a transverse axis at c.g.
M = Mach number
m = model mass
q = angular pitching velocity
q_∞ = freestream dynamic pressure
Re_d = freestream Reynolds number based on model diameter
V = model velocity relative to the media; i.e., reference point moving with the flow
X = model position relative to the media; i.e., reference point moving with the flow
α = angle of attack
$\alpha_o, \overline{\alpha_o}$ = initial and effective oscillation amplitudes
η = total angle-of-attack envelope
θ = total angle of attack, $\tan^2\theta = \tan^2\alpha + (\tan^2\psi/\cos^2\alpha)$
ρ = gas density
ψ = angle of yaw
Ω = distance oscillation frequency, rad/distance X traveled
ω = oscillation frequency, rad/sec
$(\dot{})$ = derivative with respect to time
$(\,)'$ = derivative with respect to X

Subscripts

0 = conditions at distance = 0
eff = effective
X = conditions at distance with respect to X
∞ = freestream conditions

Presented as Paper 69-105 at the AIAA 7th Aerospace Sciences Meeting, New York, January 20–22, 1969; submitted February 3, 1969; revision received August 11, 1969. This paper presents the results of one phase of research carried out at the Jet Propulsion Laboratory, California Institute of Technology, under Contract NAS 7-100, sponsored by NASA. This experimental program was successfully concluded through the cooperation of the NASA Ames Research Center (ARC) Experimental Investigations Branch and its contractor, ARO Inc. Particular recognition is due JPL employees E. Adams and W. Fife for work in test preparations and P. Jaffe for advice concerning data acquisition and analysis.

* Senior Engineer, Aerophysics Section. Associate Member AIAA.

Introduction

THE angular motions of an atmospheric entry vehicle with respect to its flight path are of concern for the following reasons: 1) amplitude-dependent aerodynamic loads must be known for proper vehicle design; 2) aerodynamic heating will vary over the vehicle's surface as a function of oscillation amplitude; and 3) operational functions such as payload or decelerator deployment or communications could be seriously affected by vehicle oscillations. The dynamic stability characteristics of several high-drag candidate atmospheric entry vehicle shapes have been investigated experimentally throughout the Mach number range. However, available data did not appear to completely define the dynamic stability characteristics in the transonic speed regime. Accurate definition of the transonic dynamic stability of these shapes was of considerable interest because the then available data suggested that a period of instability might be encountered in this region. To the author's knowledge, theoretical analysis of the dynamic stability of high-drag shapes has not been performed, and would be, at best, difficult. Consequently, emphasis has been placed on obtaining these transonic dynamic stability characteristics by experimental methods.

This paper presents the results of an experimental free-flight investigation conducted in the 6-ft × 6-ft supersonic wind tunnel at the NASA Ames Research Center (ARC), concerning the dynamic stability of 60° and 70° half-angle cones. Results demonstrating the effects of oscillation amplitude and Mach number on dynamic stability are given. In addition, computer studies of Mars entry trajectories for a 60° half-angle cone vehicle have been performed using these new experimental test data.

Free-Flight Investigation

The accuracy of experimentally obtained free-flight dynamic stability data[1] is dependent on 1) amplitude decay per cycle, and 2) number of oscillation cycles recorded during the flight. Proper model design maximizes these parameters by decreasing the size of the model while holding fixed the mass distribution. This causes the number of cycles to increase while the decay remains the same. There is, however, a lower limit to the minimum size of a model imposed by the photographic resolution and the ability to launch the model. A model diameter of 1.5 in. was chosen using these criteria.

With the model size determined, the number of cycles can be further increased by building the models with a dense core and a thin outer shell of molded, 0.02-in.-thick polystyrene plastic. In this case, the core, or ballast, was powdered tungsten, which was chosen because it, along with the model, disintegrates upon impact with the wind-tunnel structure and therefore does not damage the wind-tunnel compressor blades. The compacted ballast density exceeded that of solid lead and was packed to attain this value by the novel approach of using four grain sizes with no binder. The configurations tested are shown in Fig. 1. Models were measured for mass, center of gravity, and moment of inertia to the following accuracies: 0.1% for mass, 0.2% of the diameter for the c.g. position, and 1% for the moment of inertia. The subscripts in the model configuration designations relate to the model physical characteristics. For example, M_{60} denotes a 60° half-angle cone, N_{10} denotes a nose radius 10% of the model diameter, and E_{05} denotes an edge radius 5% of the model diameter.

The models were mounted on two triangular blades and a plate which was threaded to the piston-shaft of a pneumatic launcher.[2] The model's angles of attack at launch were adjustable and, in this experiment, were 0°, 5°, 10°, and 15°. The pneumatic pressure necessary for launching models which traveled to the upstream window edge was determined experimentally. The pneumatic launcher was mounted approximately 2 in. above and 12½ in. to the right of the tunnel center (facing upstream) on the side of the vertical pitch support strut. The minimum distance of the model from any side of the test section during flight, based on test section dimensions of 6 ft × 6 ft, was 23½ in. These distances, in relation to the small size of the models (1.5 in.), tended to minimize the possibility of pressure disturbances affecting the data. The location of the launcher was also determined so that the model release occurred approximately 8 in. from the downstream edge of the viewing area. The model was therefore free from launcher interference when it appeared in the viewing window. A typical angle-of-attack history is shown in Fig. 2. Model motion was recorded on 35-mm film using a Fastax half-frame camera. Approximately 300 film data frames were recorded for each flight at a rate of 4500 frames/sec.

Data Reduction

The raw data obtained using the free-flight techniques consist of motion picture film from which model position and angle-of-attack history in relation to the wind tunnel are determined as a function of time. The reduction of these measurements to aerodynamic coefficients is briefly described

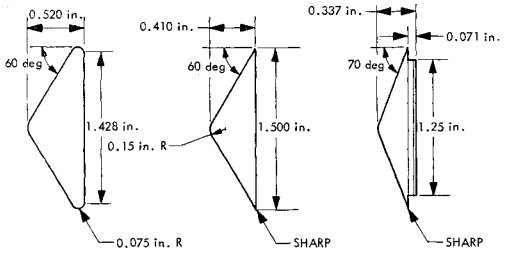

PARAMETER	CONFIGURATION		
	$M_{60}N_{10}E_{05}$	$M_{60}N_{10}E_{00}$	$M_{70}N_{10}E_{00}$
$m \times 10^3$, slugs	1.3	2.0	1.2
$I \times 10^6$ slug-ft^2	0.32	0.63	0.28
md^2/I	63	49	65
(cg/d)NOSE	0.165	0.208	0.133

Fig. 1 Free-flight model designs.

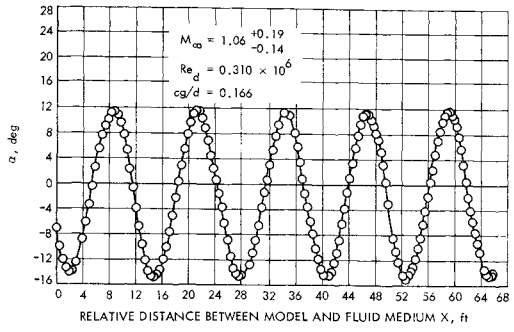

Fig. 2 Typical angle-of-attack history.

in this paper. Reference 3 presents an excellent derivation of these data reduction equations.

The coordinate system used for the reduction of data is one which references the model's position to the moving gas media; i.e., X is the distance between the model's center of gravity and a point moving with the flow and is the independent variable for the equations of motion. With the assumption of first-order linear aerodynamic coefficients, the equation for planar angular motion[3] yields an effective pitching moment slope

$$C_{m\alpha_{eff}} = -2I\Omega^2/\rho Ad \tag{1}$$

where Ω is the distance frequency of oscillation.

The dynamic stability coefficients presented in this paper were computed as follows:

$$\{\overline{C_{mq}}\}\frac{md^2}{I} = \frac{4m}{\rho A}\frac{\ln(\theta/\theta_0)}{X - X_0} + \left(C_{L\alpha} + \frac{3}{4}k\bar{\alpha}_0^2\right) - \left(C_{D_0} + \frac{K}{4}\bar{\alpha}_0^2\right) \tag{2}$$

where K and k are constants to account for nonlinear static coefficients. No correction for nonlinear pitching moment was found to be necessary for the data presented in this paper.

The dynamic stability equation[3] was derived under the assumption that the model oscillatory motion is restricted to a plane normal to the axis of the schlieren path. In this investigation, a number of flights exhibited nonplanar motion. However, only flights where the motion was very nearly confined to the vertical plane were reduced to aerodynamic coefficients, and a procedure was established to determine the total angle-of-attack (θ) history for each of these flights. Enlargements of individual film frames showing the model at peak amplitudes of oscillation were printed. Models exhibiting motion out of the vertical plane have an elliptic shaped base. From the photographic prints, the degree of ellipticity was measured, and a corresponding yaw angle ψ was computed. This angle was used to compute a total angle of attack by the equation

$$\tan^2\theta = \tan^2\alpha + (\tan^2\psi)/(\cos^2\alpha) \tag{3}$$

This total angle of attack θ was used in the dynamic stability equation [Eq. (2)], it being recognized that the assumption of a quasi-planar motion may lead to some small error in the final coefficient. However, the validity of the assumption of planar motion is supported by the quality of the test data and the good agreement of the data for flights with varying degree of yaw.

The applicability of the computed dynamic stability [Eq. (2)] was verified with an exact computer solution of the equations of motion. The static aerodynamic coefficients,[4,5] including their dependence on amplitude, and the dynamic stability coefficient reduced from flight data, were entered into the computer program and the resultant model motion computed. An example of the motion represented by the

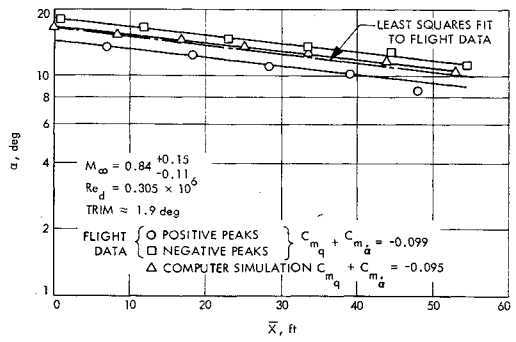

Fig. 3 Typical amplitude plot.

computed peak amplitudes is shown in Fig. 3 with the peak amplitudes of an experimental run at $M_\infty = 0.84$. The difference between the reduced damping coefficient from flight data and that resulting from the computer solution is only 4%. A similar comparison was performed for a flight of constant peak amplitude. The difference between the experimental damping coefficient (-0.038) and that of the computer solution was less than 1%. Generally, only one effective dynamic stability coefficient was obtained from a flight, but where amplitude or Mach number effects were observed to cause significant changes in the convergence or divergence of the amplitude envelope, the data were segmented and two damping coefficients were obtained. Correlation parameters for M and $\bar{\alpha}_0$ were also computed for each of these data segments.

The effective drag for each flight was obtained as follows:

$$C_D = (-2m/\rho A)[d(\ln V)/dX] \qquad (4)$$

and by numerically differentiating the slope of the lnV vs X data curve.

This mean amplitude for a flight is defined in Ref. 3 as

$$\bar{\alpha}_0^2 = \left(2\int_0^X \alpha^2 dX\right)\Big/X = (\alpha_x^2 - \alpha_0^2)/[2\ln(\alpha_x/\alpha_0)]$$

Similarly, a mean Mach number $\bar{M}$ has been used in data presentations because of the large Mach number gradients experienced by a model during its flight. This mean Mach number is defined as

$$\bar{M} = \left(\int_0^X M dX\right)\Big/X$$

and has been found to agree with M_∞ (within 1%) when the amplitude history of an entire flight was considered.

Results

The test program was designed to document the dynamic stability characteristics of configuration M_{60} N_{10} E_{00} in the transonic regime. Many repeat flights were recorded at $M_\infty = 0.95$, 1.05, and 1.15 while the initial oscillation amplitude was varied. These data formed the basis for establishing the effects of oscillation amplitude on the transonic dynamic stability. The additional complementary information obtained by testing through the Mach number range of 0.54 to 2.01 was used to determine the effect of Mach number. The test Reynolds number based on the model diameter was 0.312×10^6. However, two flights were made at $Re_d = 0.187 \times 10^6$ to indicate possible Reynolds number effects on the coefficients. The dynamic stability characteristics of a round-shoulder, 60° half-angle cone (M_{60} N_{10} E_{05}) and a 70° half-angle cone (M_{70} N_{10} E_{00}) were investigated briefly with a few flights.

All pertinent information regarding the flight test conditions together with other statistical information is presented in Ref. 6, which also cites the availability of additional experimental information.

Dynamic Stability

The effect of Mach number on dynamic stability is shown in Fig. 4. Generally, the coefficients are stabilizing at subsonic and supersonic speeds, while the transonic regime is characterized by an unfavorable (destabilizing) coefficient. The magnitude of this destabilizing trend is not as severe as has been shown by the data of Ref. 7.† Note that the c.g. locations for the ballistic range data[7] were 0.24 to 0.34 model diameters aft of the nose. Moreover, the data of this experiment are closely grouped in the transonic regime, and excellent agreement has been found to exist between data obtained for repeat conditions of Mach number and oscillation amplitude.

Dynamic stability at supersonic speeds is defined by only one data point at $M = 2.01$ (Fig. 4). However, data (unpublished) for the round-shouldered model M_{60} N_{10} E_{05} (Fig. 5) suggest a more conservative level of stability, $\overline{C_{m_q}} \approx -0.2$. These data resulted from an experimental program conducted in the JPL 20-in. supersonic wind tunnel. The tests were preliminary to the transonic program described herein, and were primarily for the purpose of developing a launcher which could assure consistent planar motion. Because of time limitations and the basic emphasis of the test, less than half the models were measured. Differences in physical properties for nominally identical models (predominantly 60° round-shouldered models with and without afterbodies) were in the range of 11%, which may account for some of the data scatter. Although it was recognized that these data do not deserve the same level of confidence as the main body of data, it was felt that, because of their relatively good repeatability, their inclusion herein was merited. The substantially constant supersonic level of stability defined by the data appears to become less stabilizing in the Mach number range $0.8 \leq M \leq 1.5$.

These data for the round-shouldered models are, in general, supported by the data of Ref. 7, particularly by the three coefficients (Fig. 5) in the Mach number range $4 < M < 6$. Krumins[7] noted a similarity in the ballistic range data resulting from round- and sharp-shouldered models

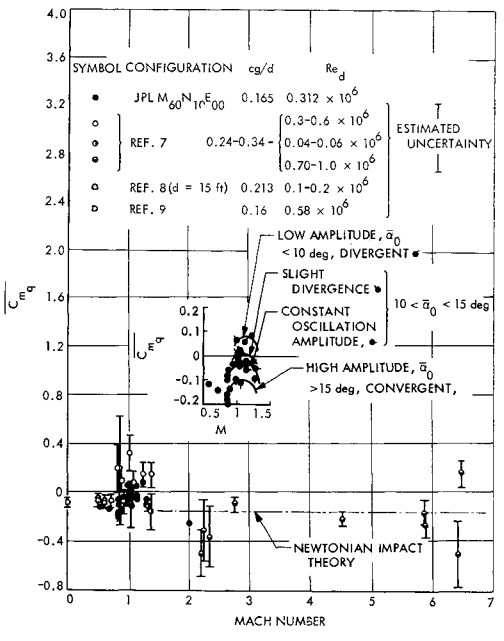

Fig. 4 Effect of Mach number on free-flight dynamic stability for sharp-shouldered 60° half-angle cone; Ref. 7 models have afterbodies.

† Data of Refs. 7–9 have been divided by 2 so that they might agree with JPL data reduction relating $\{Cm_q + Cm_{\dot\alpha}\}$ to $(\theta d/V)$ rather than $(\theta d/2V)$.

throughout a test Mach number range of 0.6 to 10.08. Newtonian impact theory more conservatively estimates supersonic dynamic stability by approximately 25%.

The definition of the subsonic dynamic stability characteristics of these shapes was not a primary objective of this investigation. However, a few flights were recorded in which the models experienced subsonic Mach numbers Those data are shown in Fig. 4. Models launched at a freestream Mach number of approximately 0.95 displayed highly convergent oscillation envelopes when slowed to $M \approx 0.9$. The trend of sharply increasing stability with decreasing transonic Mach number is the result of this effect. Figure 4 also presents data from models which were in the subsonic regime throughout the flight. A decrease in dynamic stability with decreasing Mach number is indicated by these data. The data from Refs. 8 and 9 are shown for a general comparison of planar and nonplanar data. The data of Ref. 8 are less stabilizing than the two truly subsonic data points obtained in this experiment. However, a more positive coefficient may be the result of the rearward c.g. (c.g./d = 0.22 as compared to 0.165). The subsonic spin tunnel test[9] provided data at two c.g. positions. The data point shown near $M = 0$ was obtained by adjusting the data for a forward c.g. shift that resulted in a more stabilizing coefficient. A similar correction to the data of Ref. 8 cannot be made without knowledge of c.g. effects for the full-scale configuration.

The transonic data have already been discussed generally. However, the scales used to plot all available data do not show some interesting effects clearly. The transonic dynamic stability data have therefore been replotted in the inset of Fig. 4. A close examination of the data reveals that a blanket assessment of transonic instability for these shapes is not entirely correct since four distinct types of motion related to amplitude effects are evident and have been identified by flagged symbols and fairings. Strong divergence is observed for flights in which the model's oscillation envelope was less that 10° ($\bar{\alpha}_0 < 10°$); strong convergence is observed for $\bar{\alpha}_0 > 15°$. Two types of motion are observed in the amplitude range of 10 to 15°: 1) constant oscillation amplitude and 2) slight divergence. The data for configurations M_{70} N_{10} E_{00} and M_{60} N_{10} E_{05} (Fig. 5) are not sufficient to clearly specify their transonic dynamic stability characteristics. However, the coefficient levels for these configurations are similar to those of M_{60} N_{10} E_{00} shown in Fig. 4.

Amplitude effects on the dynamic stability coefficient for the prime configuration M_{60} N_{10} E_{00} are shown in Fig. 6 for three transonic Mach numbers: 0.95, 1.05, and 1.15. The dynamic stability coefficient $\overline{C_{mq}}$ is generally destabilizing for oscillation amplitudes less than 10° and appears to become more stabilizing as amplitude is increased. A strict fairing to the data in Fig. 6 would result in a somewhat discontinuous curve suggested by the almost constant value $\overline{C_{mq}} = -0.04$

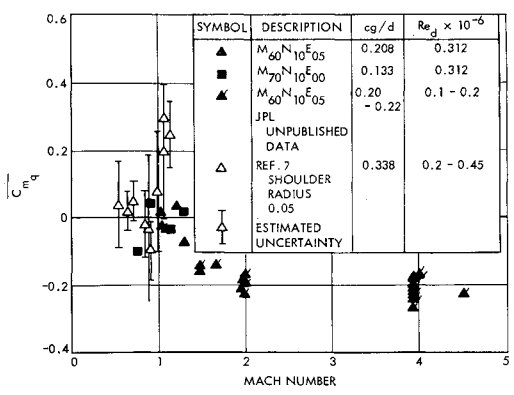

Fig. 5 Effect of Mach number on free-flight dynamic stability for round-shoulder 60° and 70° sharp-shouldered half-angle cones.

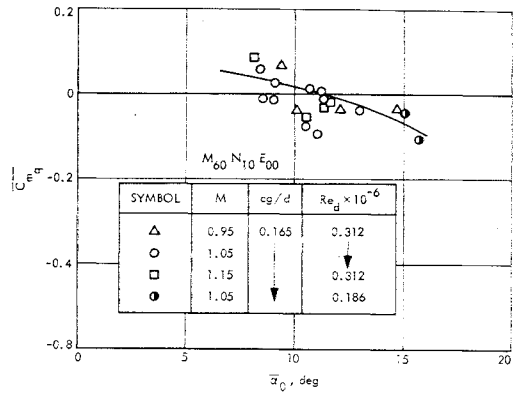

Fig. 6 Effect of oscillation amplitude on dynamic stability.

computed from flights at constant oscillation amplitude. However, it is unlikely that such a discontinuous fairing would represent a variation in amplitude effect on dynamic stability. Consequently, a smoother fairing has been applied to the data until more definitive results are available. It should be noted that although data were not obtained for $\bar{\alpha}_0 < 7°$, knowledge of the dynamic stability in this low-amplitude range may be somewhat academic. Extremely destabilizing coefficients, should they exist, have only resulted in model amplitude divergence to amplitudes where the coefficients are definitely stabilizing and clearly defined.

Drag and Static Stability

While the primary objective of the experimental program was to obtain dynamic stability data, interesting and perhaps useful free-flight drag and static stability data were also obtained as a by-product of the dynamic stability investigation. Static data are necessary for the reduction of the dynamic damping data to aerodynamic coefficients, and these free-flights data are of significance because they are free from support interference. Sting-support interference has been found to be significant for these shapes in the transonic regime.[4]

The transonic drag rise curve (Fig. 7) was obtained by plotting the effective drag for each flight. The drag coefficient $C_{D_{\text{eff}}}$ was computed using the slope of a linear least-squares curve fit to the (ln V) data described in Eq. (5). Since the oscillation amplitude had little effect on C_D, the data (see Fig. 8 and Ref. 4) in the figure also summarizes C_{D_0}. The data for the three configurations tested are consistent and show good repeatability in the transonic regime. Repeat points which are indistinguishable from each other are noted by a flagged symbol. It should be noted that the transonic drag rise portion of the two curves are different. Detailed drag vs Mach data were generated from distance-

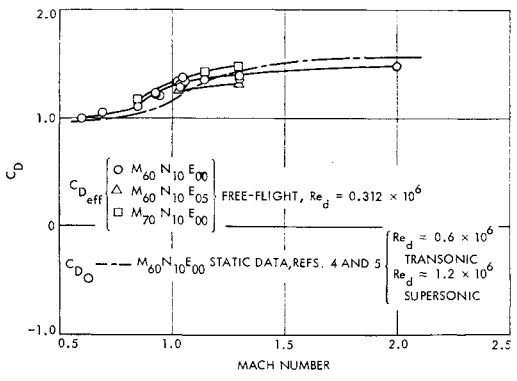

Fig. 7 Effect of Mach number on free-flight drag.

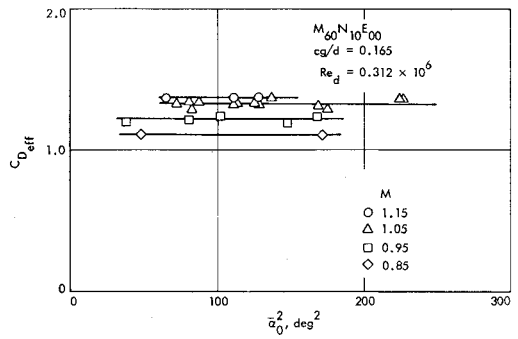

Fig. 8 Effect of oscillation amplitude on drag.

time histories to check the accuracy of the "effective" drag coefficient. The results were similar to the free-flight drag shown, indicating no error in the data reduction. The early free-flight drag rise may be attributed to several conditions. Model acceleration, sting interference in the static data, Reynolds number difference and possible wind-tunnel blockage (static data) should be considered in investigations of the phenomenon. Acceleration effects might be investigated by testing light models at high dynamic pressure and heavy models at low dynamic pressure.

The dependence of static stability C_{m_α} on Mach number is shown in Fig. 9. The configurations are all statically stable for the test amplitude range, with stability increasing with decreasing Mach number. The sharp-shoulder model (M_{60} N_{10} E_{00}) is more stable than the other configurations. However, the effects of configuration and center of gravity on C_{m_α} were not investigated and therefore are not immediately separable from the relative curve displacements. The effects of oscillation amplitude on C_{m_α} has been indicated in a general manner by grouping the data into one of three amplitude ranges designated by the flagged symbols.

Flow Visualization

The photographic data obtained in this experiment not only provide the quantitative results to describe the model's time-motion history, but also provide excellent documentation of the flowfield. A sequence of motion picture frames (not consecutive) has been assembled in Fig. 10 to show the major developments of the flowfield as the model traverses the transonic Mach number range. Frame 70 shows a typical picture of the flow about these shapes at transonic Mach numbers. The bow shock wave is detached, and a wake of increasing and then decreasing downstream diameter is observed, followed by the usual recompression wake shock. As the Mach number experienced by the model decreases

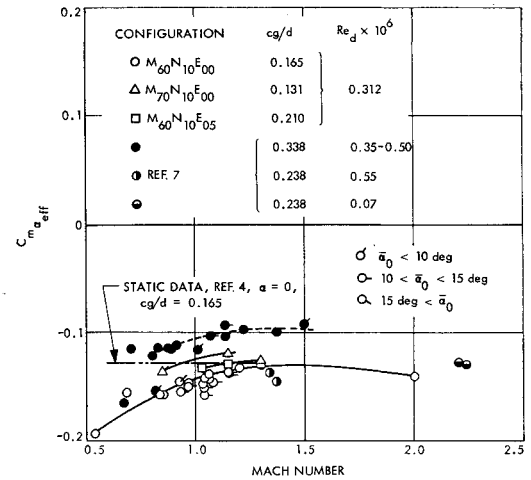

Fig. 9 Effect of Mach number on static stability.

in succeeding frames, the bow shock wave becomes further detached from the model and the wake becomes less convergent. The wake recompression shock adjusts to these changes in wake shape and also becomes almost perpendicular to the direction of the flow. Dramatic transients in the wake are revealed in frames 170 through 210, in which the recompression shock becomes less distinct. The model actually passes through the remaining weak disturbances in later frames (not shown). Although much of the interesting dynamic history of the wake is lost by fixing the motion picture history in still photographs, the flow detail necessary to investigations of possible influences of the wake on transonic dynamic stability for many shapes is clearly indicated.

Application of Experimental Data

The dynamic stability coefficient obtained in this experiment is an effective constant correlated with an effective angle of attack $\bar{\alpha}_0$. However, it is the "local" dynamic stability, correlated with the local angle of attack, that is used in computer trajectory simulations. One method to determine the dynamic stability coefficient as a function of local angle of attack is to assume a functional form which, when integrated, gives the same effective experimental coefficient (more than one function could be possible). The choice of this solution can become quite difficult when a complete entry trajectory with its corresponding changes in θ over wide Mach number variation is studied. This solution must be formulated with the knowledge that the local dynamic stability coefficient could be a function of a number of variables, θ, θ', θ_0, etc. Only the following equality[10] must be preserved:

$$(\overline{C_{m_q}})_{\text{eff}} \int_{-(\theta_0-\delta\theta)}^{+\theta_0} \theta' d\theta = \int_{-(\theta_0+\delta\theta)}^{+\theta_0} (\overline{C_{m_q}})_{\text{local}}\, \theta' d\theta$$

A local dynamic stability solution in the transonic regime will be difficult to obtain for two reasons: 1) transonic dynamic stability is apparently nonlinear by inference from the amplitude effects, and 2) it is not clear that the data resulting from two dissimilar types of motion (planar and nonplanar) are identical. More understanding of these areas will be required before the "local" dynamic stability can be defined for these shapes.

In the following discussion, an alternate method for computing the planar amplitude oscillation of an entry capsule is used to study briefly the effect of these new test data. An angle-of-attack history, which has been computed or assumed is used to synthesize a $\{\overline{C_{m_q}}\}_{\text{eff}}$ history compatible with θ and Mach number using experimental amplitude-dependent data. This dynamic stability curve should be a function of Mach number only. A new trajectory is computed using the previously synthesized curve, and (as previously) a new dynamic stability history as a function of Mach number is

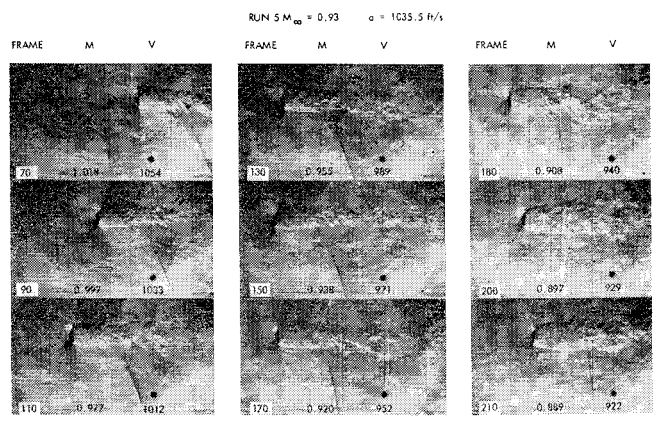

Fig. 10 Key flowfield events.

determined from this trajectory. The iteration process is continued until the amplitude solution converges with the presupposed dynamic stability history. This $\overline{C_{mq}}$ vs Mach number curve represents the solution for the particular initial conditions chosen for the trajectory, entry capsule, and atmosphere. Further iterations are necessary for changes in these conditions because a variation in these parameters will result in a change in the oscillation envelope.

The vehicle characteristics used in the following computer simulations are given in Fig. 11. The trajectories used a 20-mbar surface pressure atmosphere intended to represent the upper limit of Martian atmospheres. The static aerodynamic coefficients used in the computer program were drawn from Refs. 1 and 5 and from unpublished data from experiments conducted at the NASA Langley Research Center. Computation was begun at an altitude of 8×10^5 ft, with a velocity of 23×10^3 fps and an entry angle of 50°.

Figure 11 presents the vehicle's angle-of-attack envelope vs Mach number for the Mars entry trajectories. The corresponding Mach-number-dependent dynamic stability curves are shown in Fig. 12. The dashed curve (Fig. 12) was originally a conservative (unfavorable) estimate of the dynamic stability of the 60° half-angle cone configuration based on Newtonian theory and some of the experimental data presented in this report. No oscillation amplitude dependence was assumed in the dashed curve.

Curve A in Fig. 11 represents the envelope for the terminal portion of the entry trajectory, including the transonic-subsonic regimes. Because of the negative stability coefficient (Fig. 12, dashed curve), the vehicle is well damped and the envelope is less than 1° above an altitude of 97,000 ft at $M = 2$. Divergence to $\eta = 2.7°$ may be observed in the transonic regime and is the result of the destabilizing coefficient described for these speeds. Even after experiencing such a large change in the dynamic stability

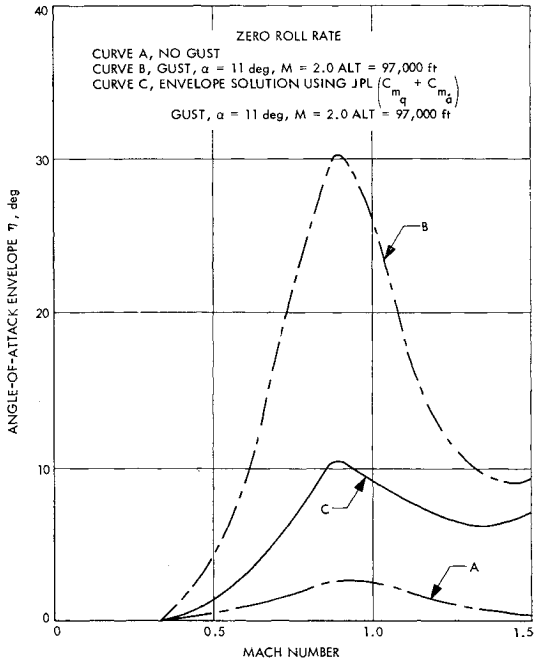

CAPSULE						ATMOSPHERE				
m, slugs	d, ft	$\frac{X_{cg}}{d}$	I_x, slug-ft^2	I_y, slug-ft^2	m/C_DA, slug/ft^2	T_0, °R	ρ_0, slug/ft^3	P_0, mbar	g, ft/sec^2	β, ft^{-1}
5.815	6.5	0.19	13.37	8.03	0.117	495	5.3×10^{-3}	20	12.3	2.12×10^{-5}

Fig. 11 Low-speed angle-of-attack envelopes, Mars entry.

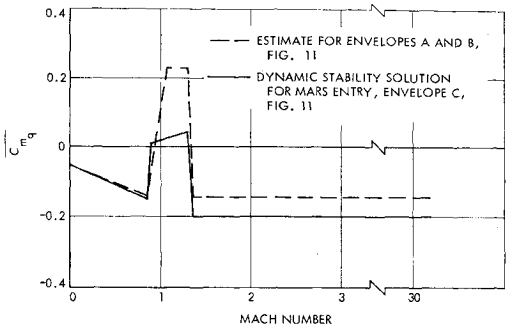

Fig. 12 Variations of the dynamic stability coefficient.

coefficient, the vehicle angle-of-attack envelope cannot be judged critical in the sense of tumbling. The envelope is shown only for $M < 1.5$; it is rather uninteresting and well damped at supersonic and hypersonic speeds.

To amplify the transonic divergence, a step function gust was introduced in curve A (Fig. 11) at $M = 2$, which resulted in an angle of attack of approximately 11°. The resultant angle-of-attack envelope (using the dashed curve for $\overline{C_{mq}}$ in Fig. 12) is shown in Fig. 11, curve B. The envelope slightly exceeded 30° at $M = 0.8$. Using this envelope and the previously described iteration process, a solution was found for η and $\overline{C_{mq}}$ as a function of Mach number based on the amplitude-dependent damping data presented in this paper. The result for the envelope is shown in curve C in Fig. 11. No alarming transonic divergence results from the dynamic stability solution shown in Fig. 12 (solid curve).

Summary of Results

A parametric investigation of the transonic dynamic stability characteristics of one 70° and two 60° half-angle cones has been conducted. Other than configuration, parameters considered were oscillation amplitude and Mach number. The following may be concluded from test results and computer studies of the oscillation amplitude history of a Mars entry capsule.

1) The 60° and 70° half-angle cones exhibit less dynamic stability in the transonic regime compared with levels at subsonic and supersonic speeds. However, this destabilizing trend is oscillation-amplitude-dependent and occurred generally for flights at $\bar{\alpha}_0 < 10°$. Constant oscillation amplitudes were observed for the amplitude range $10 < \bar{\alpha}_0 < 15°$ and decaying amplitudes at higher angles. Further investigations should include a more detailed look at one configuration and the effects of spin and scaling parameters such as c.g., dimensionless frequency, and Reynolds number. Any investigation should be restricted to the use of free-flight techniques (wind tunnel, ballistic range, or full-scale flights) to insure valid data. Any evaluation of sting-interference effects should be paralleled by free-flight data. The data of Refs. 7, 8, and 9 have been presented together with the data of this experiment. However, it remains to be shown whether these data resulting from dissimiliar types of motion can be directly compared or, even more important, whether a "local" coefficient representing all of these data can be synthesized.

2) Free-flight drag data are in reasonable agreement with static, sting-supported model data at subsonic and supersonic speeds and ballistic range data at $M \approx 2$. The free-flight drag rise is, however, different from the static curve in that it begins at a lower Mach number. Investigations of this difference should consider model acceleration sting interference, Reynolds number, and possible static test tunnel blockage effects. As expected, drag sensitivity to oscillation amplitude is not discernible for $\bar{\alpha}_0 < 15°$. Static stability data are consistent both internally and with other reported

free-flight data and show a trend of increasing stability with decreasing Mach number.

3) The free-flight technique has been successfully used in a continuous-flow transonic wind tunnel and has important advantages compared to other free-flight techniques. Model characteristics may be optimized to emphasize the desired data under controlled initial conditions, angle of attack, roll, and yaw. These important advantages are supported by the large number of data points (approximately 300), defining model angular motion history and flowfield characteristics. It is suggested that a biplanar mirror system developed for use with a conventional wind tunnel[11] would extend the present planar capability to the study of nonplanar motion of spinning models. The comparison of planar and nonplanar motion under the same test conditions would then be practical.

4) The data presented herein were used in a six-degree-of-freedom computer simulation. No alarming motions, such as tumbling or even large amplitude of oscillation, were observed, even when the hypothesized vehicle experienced a gust-induced angle of attack of 11° at $M = 2$ and 97,000-ft altitude.

References

[1] Dayman, B., Jr., "Free-Flight Testing in High-Speed Wind Tunnels," AGARDograph 113, NATO-AGARD, Paris, May 1966.

[2] Holway, H., Herrera, G., and Dayman, B., Jr., "A Pneumatic Model Launcher for Free-Flight Testing in a Conventional Wind Tunnel," TM 33-177, July 30, 1964, Jet Propulsion Lab., Pasadena, Calif.

[3] Prislin, R. H., "Free-Flight and Free-Oscillation Techniques for Wind Tunnel Dynamic Stability Testing," TR 32-878, March 1966, Jet Propulsion Lab., Pasadena, Calif.

[4] Marko, W. J., "Static Aerodynamic Characteristic of Three Blunted Sixty-Degree Half-Angle Cones at Mach Numbers from 0.60 to 1.30," TR 32-1298, July 1968, Jet Propulsion Lab., Pasadena, Calif.

[5] Walker, B. and Weaver, R. W., "Static Aerodynamic Characteristics of Blunted Cones in the Mach Number Range from 2.2 to 9.5," TR 32-1213, Dec. 1967, Jet Propulsion Lab., Pasadena, Calif.

[6] Marko, W. J., "Transonic Dynamic and Static Stability Characteristics of Three Blunt Cone Planetary Entry Shapes," TR 32-1357, July 1969, Jet Propulsion Lab., Pasadena, Calif.

[7] Krumins, M. V., "Drag and Stability of Mars Probe/Lander Shapes," *Journal of Spacecraft and Rockets*, Vol. 4, No. 8, Aug., 1967, pp. 1052–1057.

[8] Whitlock, C. H. and Bendura, R. J., "Dynamic Stability of a 4.6-Meter-Diameter 120-deg Conical Spacecraft at Mach Numbers from 0.78 to 0.48 in a Simulated Martian Environment," TND-4858, May 1968, NASA.

[9] Bendura, R. J., "Low Subsonic Static and Dynamic Stability Characteristics of Two Blunt 120-Deg Cone Configurations," TND-3853, 1967, NASA.

[10] Jaffe, P., "A Generalized Approach to Dynamic-Stability Flight Analysis," TR 32-757, July 1965, Jet Propulsion Lab., Pasadena, Calif.

[11] Prislin, R. H. and Holway, H. P., "A Wind Tunnel Free-Flight Testing Technique for Nonplanar Motion of Spinning Models," AIAA Paper 66-774, Los Angeles, Calif., 1966.

DECEMBER 1969 J. SPACECRAFT VOL. 6, NO. 12

Characteristics of Atmospheric Turbulence as Related to Wind Loads on Tall Structures

GEORGE H. FICHTL,* JOHN W. KAUFMAN,† AND WILLIAM W. VAUGHAN‡

NASA Marshall Space Flight Center, Ala.

An engineering boundary-layer wind model based on data collected at the NASA 150-m meteorological tower facility at the Kennedy Space Center, Fla. is presented. Hourly peak-wind profiles of the form $u(z) = u_{18}(z/18)^k$ and climatological hourly peak-wind statistics at the 10-m level are used to specify design peak-wind profiles, where $u(z)$ is the hourly peak wind speed at height z in meters, u_{18} is the 18-m level peak-wind speed, and $k = bu_{18}^{-3/4}$. The parameter b is normally distributed. The relationship between the instantaneous extreme and the peak-wind profiles for time periods up to ten minutes is examined. The use of the peak-wind profile concept in design studies could produce overestimates in drag loads. Empirical formulas are obtained to estimate the gust factor $G(z) = u(z)/\bar{u}(z)$, where $\bar{u}(z)$ is the time mean wind at height z associated with a specified averaging time. The gust factor is a monotonically increasing function of the averaging time and a decreasing function of z. For daytime conditions the gust factor is a monotonically decreasing function of u_{18}, while for nighttime conditions, it is a monotonically increasing function of u_{18}. A spectral model of the longitudinal and lateral components of turbulence for the neutral boundary layer (high-wind speeds) is presented. The model accounts for the vertical variation of turbulence power spectra.

Nomenclature

b = parameter that characterizes the statistics of k
C_p = specific heat of dry air at constant pressure
C = empirically determined parameter that occurs in formulas of the longitudinal and lateral spectra
f = $nz/\bar{u}$
f_m = value of f associated with peak of logarithmic spectrum

Received March 28, 1969; revision received August 20, 1969. The authors wish to thank Mr. O. E. Smith for his interest, helpful comments, discussion, and use of Fig. 1.

* Scientific Assistant.

† Chief, Atmospheric Dynamics Branch.

‡ Chief, Aerospace Environment Division, Aero-Astrodynamics Laboratory. Associate Fellow AIAA.